Tomorrow's Surgery

Anita M. Flynn, K.R. Udayakumar, David S. Barrett and James D. McLurkin

January 29, 1995

Abstract

Surgical procedures have changed radically over the last few years due to the arrival of new technology. What will technology bring us in the future? This paper examines a few of the forces whose timing are causing new[1] *ideas to congeal from the fields of artificial intelligence, robotics, micromachining and smart materials.*

Intelligence systems for autonomous mobile robots can now enable simple insect level behaviors in small amounts of silicon. These software breakthroughs coupled with new techniques for microfabricating miniature sensors and actuators from both silicon and ferroelectric families of materials offer glimpses of the future where robots will be small, cheap and potentially very useful to surgeons.

In this paper we relate our recent efforts to fabricate piezoelectric micromotors in an effort to develop actuator technologies where brawn matches to the scale of the brain. We discuss our experiments with thin film ferroelectric motors 2 mm in diameter and larger 8 mm versions machined from bulk ceramic and sketch possible applications in the surgical field.

1 Intelligent Machines

Today surgeons routinely remove organs with minimally invasive procedures that were unheard of just a few years ago. What will be next?

It seems clear that more dextrous manipulators and better visualization tools will be the upcoming items on the agenda. After that, perhaps placing the intelligence also at the point of interest? While the idea of an autonomous robot running amuck inside the human body is a scary thought, it certainly is plausible to imagine beginning with low level reflexive actions for locomotion or manipulation carried out autonomously, while a fiber-optic cable is tethered to a surgeon for observation and direction.

At the MIT Mobile Robotics Laboratory, new approaches in artificial intelligence have led to novel intelligence architectures used on robots which explore, build maps, have an onboard manipulator, walk, interact with people, navigate visually and learn to coordinate many conflicting internal behaviors [1]. This type of control system, known as a subsumption architecture, is implemented as a distributed layered network of augmented message-passing finite state machines [2] and enables very tight loops between perception and action to be maintained in a mobile robot's dynamically changing world.

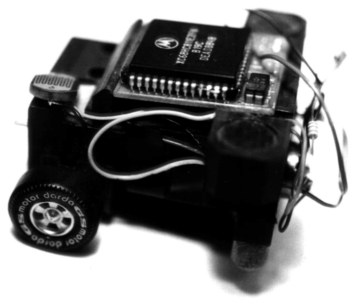

Figure 1: Squirt is an autonomous robot measuring 2.5 cm on a side, carrying onboard computer, sensors, motor and batteries.

Figure 1 illustrates Squirt, the smallest simplest robot built under this paradigm [3]. Two microphones and a light sensor trigger insect style behaviors of hiding in the dark and moving towards noise. The subsumption program endowing Squirt with these capabilities fits in a very lean 1300 bytes of code.

Unfortunately, Squirt's lone DC gearhead motor grants only one degree of freedom; forwards or back and turn (when a clutch on the rear axle allows one wheel to slip). While an entire computer with accompanying software, sensors and batteries can fit into a Squirt-sized package, it is difficult to include very many motors for finer dexterity.

With the advent of silicon micromachining techniques in which electrostatic motors the size of a human hair can be etched in place on the surface of a silicon chip [4], the thought arose to pattern an entire robot on a chip [5]; sensors, subsumption control system compiled to the gate level, actuators and solar cells, as all components

[1]Support for this work wasprovided in part by the Gnat Robot Corp., in part by the MIT Lincoln Laboratory Advanced Concepts Committee and in part by the Advanced Research Projects Agency under Ft. Dietrick contract DAMD17-94-C-4102.

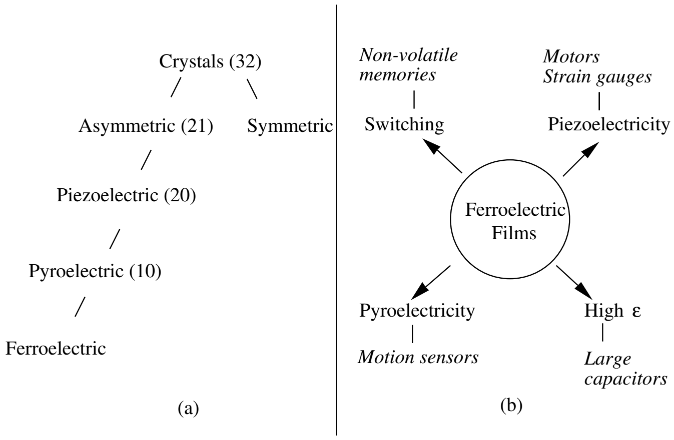

Figure 2: (a) Subsets of asymmetric crystal classes exhibit the effects of piezoelectricity, pyroelectricity and ferroelectricity. (b) These effects can be used to create capacitors, memories, sensors and actuators.

could be fabricated in silicon. Resulting machines could be printed in the same manner as integrated circuits and mass produced in low cost batch fabrication lots, enabling *cheap disposable robots.*

Unfortunately, the problem here is that silicon electrostatic motors have a number of drawbacks for small robots. They typically spin at high speeds with very small torque and are hard to scale up, necessitating that the rest of the system be scaled down to their domain.

We would be interested in slightly larger, but still small motors which would be compact, direct-drive, cost-effective and able to couple useful torque to a load for the purpose of creating robots that act as autonomous sensors and manage to find their way into hard to reach places.

A number of technologies look promising here such as magnetic or electrostatic wobble motors [6], polymer gels for artificial muscles [7] and piezoelectric ultrasonic motors [8]. Our investigations are focused on scaling down ultrasonic motors and attempting to microfabricate them using new ferroelectric thin films of lead zirconate titanate (PZT) [9].

1.1 Smart Materials

Figure 2 illustrates why we find stepping outside the bounds of traditional silicon microprocessing and adding thin film PZT to be intriguing for microfabricated robots. While ferroelectric materials such as PZT have high dielectric coefficients ($\epsilon = 1300\epsilon_o$) and a hysteretic relationship between polarization and electric field making them excellent materials for capacitors and non-volatile memories, ferroelectrics also exhibit pyroelectric and piezoelectric effects. The pyroelectric effect is a change in charge density when the material is uni-

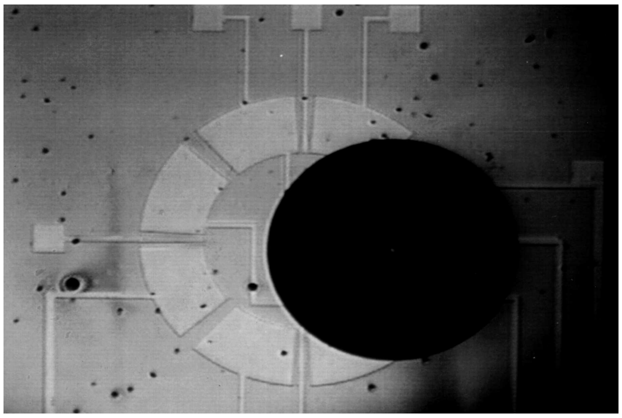

Figure 3: Thin film PZT is used to fabricate piezoelectric micromotors.

formly heated and the piezoelectric effect is a similar response when the material is stressed. The pyroelectric and piezoelectric effects can be utilized to create motion sensors and force sensors, respectively. The piezoelectric effect can be applied in the reverse manner where an applied voltage induces the material to deform. This latter characteristic is the basis of piezoelectric actuators. Thus many components of a robot can be fabricated with the addition of this one material to a traditional silicon process.

1.2 The Piezoelectric Effect

Piezoelectricity describes the first order (linear) coupling between the dielectric and elastic phenomena. For an anisotropic, homogeneous solid, under isothermal conditions, and negelecting the magnetic field effects, the components of the elastic strain tensor, x_{ij}, are given by the following relation:

$$x_{ij} = s^E_{ijkl}X_{kl} + d_{ijk}E_k + \text{ higher order terms}$$

where X_{kl} and E_k are the components of the stress tensor and the electric field vector, respectively. The s^E_{ijkl} coefficients are the components of the elastic compliance tensor measured at constant electric field. The components d_{ijk} of the piezoelectric tensor define the electromechanical coupling. Neglecting higher order terms, if a static electric field is applied to a piezoelectric material that is free to change shape, the total stress X is zero and the equation reduces to $x_{ij} = d_{ijk}E_k$. The piezoelectric term thus relates the mechanical strain developed in a material as a consequence of the electric field applied to the material. d is thus called the strain coefficient, and the equation defines the converse piezoelectric effect. Alternatively, for a linear, anisotropic, homogeneous, polarizable solid, the components of the dielectric displacement vector D_i are given by the relation:

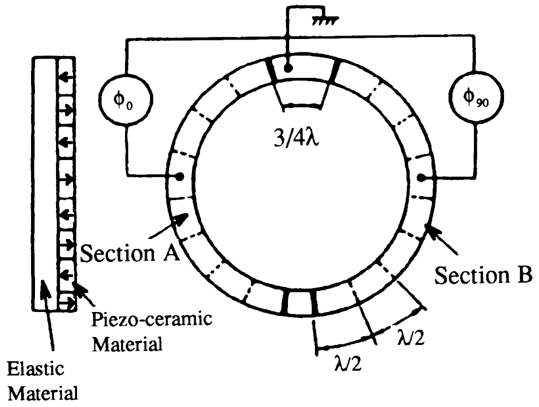

Figure 4: Two standing wave offset by $\frac{\lambda}{4}$ and driven 90 degrees out of phase combine to form a traveling wave of deformation.

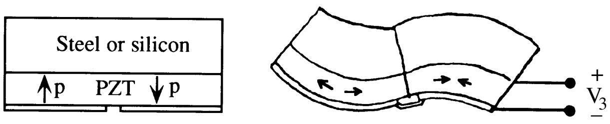

Figure 5: Neighboring electroded segments, if alternately poled, will strain oppositely when driven with a common voltage.

$$D_i = d_{ijk}X_{jk} + \epsilon_{ij}^X E_j + \text{ higher order terms}$$

where ϵ_{ij}^X are the components of the dielectric permittivity tensor measured at constant stress. Again, neglecting higher order terms, if a stress is applied to the piezoelectric material that is short-circuited, the total electric field across the material is zero, and the equation above becomes $D_i = d_{ijk}X_{jk}$. In this case, the piezoelectric term relates the charge developed on the material's surface upon application of stress. The d coefficient is then called the piezoelectric charge coeffiecient and the corresponding electromechanical coupling is known as the direct piezoelectric effect.

1.3 Motors

Figure 3 is a photograph of a 2 mm thin film PZT micromotor structure fabricated on a 1 μm thick silicon nitride membrane. A small plano-convex glass lens placed down upon the substrate is used as the rotor and spins at 100–300 rpm for 90 kHz excitation at 5 V [10, 11].

These initial structures validated the films as useful for actuators but did not incorporate any bearings or means for coupling power out. Larger ultrasonic motors which are commercially popular in Japan [12, 13, 14] use bulk ceramic PZT in an annular ring configuration as shown in Figure 4. Figure 5 illustrates the basic principles behind a ring-type ultrasonic motor. Bulk ceramic PZT is bonded in segments onto an elastic body such as steel. A large electric field is applied to each segment oppositely to induce an initial polarization direction. When all segments are wired together and driven with a common voltage, neighboring segments strain in opposing directions causing the structure to buckle. An oscillating applied voltage converts the buckling pattern into a standing wave of mechanical deformation.

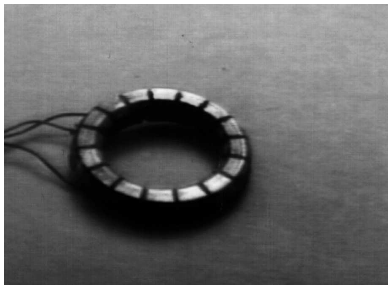

Figure 6: The stator of an 8 mm ultrasonic motor is made from bulk ceramic PZT bonded onto a ring of steel.

Ring-type ultrasonic motors superimpose two standing waves which are a quarter wavelength out of phase in both space and time (Figure 4) to generate a traveling wave of bending. A traveling wave has the property that any point on the surface of the beam moves in an elliptical trajectory perpendicular to the plane of the ring. A rotor pressed against the surface is then propelled along through friction. These types of motors consequently generate high torque at low speeds and do not require gears.

Presently, we are experimenting with smaller versions of bulk ceramic ultrasonic motors, but which are larger than the thin film structures on membranes. Figure 6 shows a stator of an ultrasonic motor 8 mm in diameter.

While bulk ceramic PZT requires high voltages (typically 50–100 V) to achieve the required field strengths, thin film PZT is 500 times thinner and can run directly from batteries without recourse to DC-DC converters. Since the motors can also perform without gears in a direct-drive fashion, significant weight can be reduced for a mobile robot. Figure 7 shows our thin film PZT stators, of the same dimensions as the ring-type stator of Figure 6, which have been microfabricated in a new laser-based process which requires zero masks and no wet etching, offering potential for low cost fabrication.

2 Mini Robots

If small compact useful motors were available, what kinds of systems could we build and what orders of speeds and torques would we require? Essentially, we would like motors of the same size scale as the sensors we use today. This is especially true for robots whose

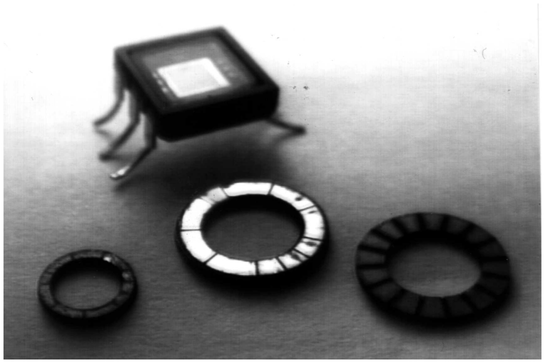

Figure 7: Laser processed ultrasonic motor stators are comprised of layers of oxide, titanium, platinum, PZT and gold, on a silcon substrate.

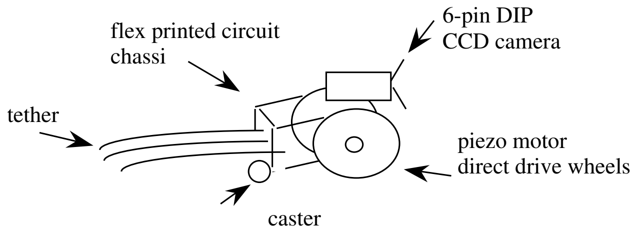

Figure 8: Two 8 mm piezomotors with rubber O-rings wrapped around the rotors could serve as tires for a two-degree-of-freedom steerable cart.

job is to collect information as opposed to heavy-lift assembly operations. We now sketch a number of plausible systems.

2.1 A One Cubic Centimeter Camera-Toting Cart

Using the strategy of batch fabricating half a motor and hand assembling the rest, with 8 mm motors it is conceivable to build a very useful system, a small teleoperated robot propelling a camera. On earlier robots we have used 192×165 serial CCD imagers in 6-pin packages (manufactured by Texas Instruments and shown in Figure 7). This camera would be roughly the same size as our motor.

We propose to use two small direct drive 8 mm motors surface-mounted onto a flexible printed circuit board which bends to form the chassis of the cart as shown in Figure 8. Small rubber O-rings are pushed onto the rotor and serve as tires for the piezomotor-driven wheels. Wires run from the stators to a connector for the tether. The camera chip and small lens mount on a top flap of the flex printed circuit and a caster on the bottom provides a three-point stance. The entire package should fit in roughly one cubic centimeter and will contain twice as many degrees of freedom as Squirt.

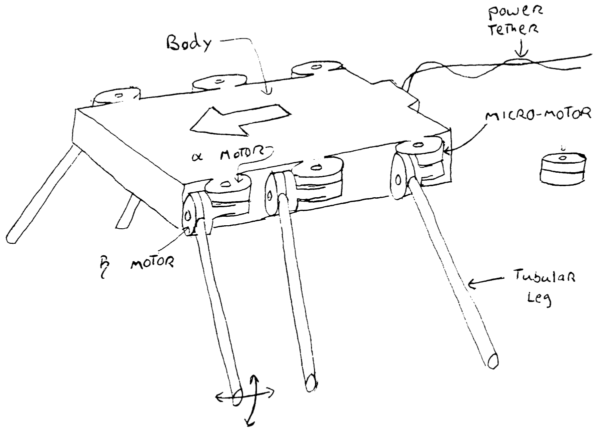

Figure 9: The high torque, low speed characteristic of a piezomotor means that it can be used in a direct drive fashion which is convenient for robots, especially those with many degrees of freedom such as this six-legged walker.

2.2 Micro Crawlers

Other means of locomotion besides wheels can be useful for microrobots. Here we show a simple design and give torque requirements for a six legged walker incorporating twelve piezoelectric micromotors (Figure 9).

Each hip contains two motors marked α and β, (for advance and balance respectively). The robot walks in a tripod gate with power coming from offboard via a tether. The β motors must be able to support $\frac{1}{3}$ the total bug weight and lift the leg clear of the ground. The α motors carry a much lighter load, and so the same β motor design will suffice. What sorts of torques and power supplies are required here? Table I lists dimensions and materials for one specific bug design.

Table I. Bug parameters and torque requirements.

Body	2.5 cm$\times$6.4 mm$\times$3.2 mm
(Aluminum)	ρ = density = $2706\frac{kg}{m^3}$
Motors	3.2 mm dia.$\times$3.2 mm long
(Silicon)	ρ = density = $2596\frac{kg}{m^3}$
Legs	1.3 mm dia.$\times$9.5 mm long
(Steel)	ρ = density = $7731\frac{kg}{m^3}$
Leg weight	0.9 g
Total weight	2.07 g
Torque – support	4.6×10^{-4} kgf–cm
Torque – lifting	4.5×10^{-5} kgf–cm
Power – lifting $\frac{1rad}{s}$	4.5×10^{-5} W/motor
Power – total	1.35×10^{-4} W
Current at 5 V	2.7×10^{-5} A

In a tripod gate, three legs are in the air at any one

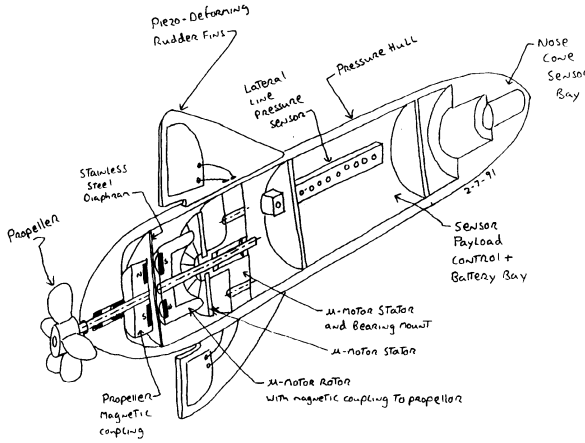

Figure 10: A 2.5 cm long submarine robot incorporates a piezoelectric micromotor for propulsion.

time. Total weight includes the body, six motors and three legs. The maximum torque required for each of the three motors to support one third of the total body weight is calculated as the legs touch the ground at a 45 degree angle from the body. Power requirements per motor are calculated as though providing this torque at the rate of one radian per second. Table I then gives us some feeling for the ballpark torques and power supplies a small robot might require. In this case, required torque is 4.6×10^{-4} kgf-cm.

2.3 Micro Submersibles

An underwater robot's propulsion system might be similar to that portrayed in Figure 10. A floating or submersible robot would be quite a bit easier to build than a walker because a neutrally buoyant swimmer can carry weight equivalent to the weight of the water it displaces.

In order to calculate the types of torques a small submarine would need let us assume the submarine is cylindrically shaped with a diameter of 5 mm and a length from nose to end of 25 mm. We will also assume that the motor is cylindrically shaped 4 mm in diameter and 3 mm long.

$D_s = 5$ mm
$L_s = 25$ mm
$\rho_w =$ density of water $= 998\frac{kg}{m^3}$
$\nu_w =$ viscosity$= 1.0 \times 10^{-6}\frac{m^2}{\text{sec}}$
$D_m = 4$ mm
$L_m = 3$ mm
$\rho_{si} =$ density of silicon $= 2340\frac{kg}{m^3}$

Weight of water displaced $= \frac{\pi D_s^2}{4} L_s \rho_w = 0.49$ g
Weight of the motor $= \frac{\pi D_m^2}{4} L_m \rho_{si} = 0.088$ g
Weight of payload allowed $= 0.402$ g

The drag force in the water is a function of the coefficient of drag, the density of the water, the velocity of the submarine and its cross-sectional area.

$$D_F = C_d \left(\frac{\rho_w V^2 A}{2}\right)$$

$$C_d = \text{coef drag} = 0.44\frac{D_s}{L_s} + 0.16\frac{L_s}{D_s} + 0.016\sqrt{\frac{D_s}{L_s}}$$

$$\text{where } 1 \leq \frac{L_s}{D_s} \leq 10 \qquad \text{Re} \leq 2\times10^5 \quad \text{Re} = \frac{VD_s}{\nu_w}$$

Let us assume a velocity of the submarine of $V = 10\frac{mm}{\text{sec}}$.

$D_F = 1.72 \times 10^{-7}$ N
Re $= 10$ (regime is correct for coeff. of drag)

Now we calculate the thrust produced by the propeller. For steady state translation, the thrust must just offset the drag. Assume a propeller diameter of 5 mm.

$d =$ diameter of propeller $= 5$ mm
$Q =$ shaft torque
$T =$ axial thrust
$N =$ angular velocity of propeller
$V =$ free stream velocity
$P =$ propeller pitch
$J =$ advance ratio $\frac{V}{Nd}$
$\eta_p =$ propeller efficiency $= \frac{VT}{2\pi NQ}$
$\frac{P}{d} =$ propeller pitch to diameter ratio

For steady state translation, $T = D_F$.

$$\eta_p = \frac{VD_F}{2\pi NQ}$$

$$Q = \frac{VD_F}{2\pi N\eta_p}$$

Assuming that the propeller turns at $N = 100$ rpm, the advance ratio J is approximately 0.2. Propeller characteristics are given in terms of propeller efficiency vs. advance ratio for a given propeller pitch to diameter ratio. For this advance ratio and a $\frac{P}{d}$ of 0.6, η_p is known to be 0.2. Now we can calculate the shaft torque and motor power.

$Q = 1.3 \times 10^{-10}$ Nm$= 1.3 \times 10^{-9}$ kgf-cm
$P_m = Q \times N =$ motor power $= 1.4 \times 10^{-9}$ W

This tells us that the torques and power requirements for neutrally bouyant systems can be quite small. This is good news for medicine, because robotics for fluid filled tubes in the human body is just ocean engineering on a tiny scale.

3 The Future

A revolution has occurred in surgery in the last few years but the best is yet to come. Laparoscopic and endoscopic tools extend the doctor's hands and eyes, but for the most part the surgeon plays the part of the solo performer in a quartet. Perhaps in the future, his or her role will be that of a conductor of an orchestra, where a team of micro interns find their way through the maze of tubes in the body, carrying sensors and tools and freeing the surgeon of the taxing burden of negotiating every low level activity.

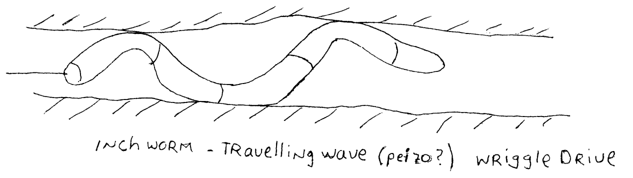

Figure 11: A crawling robot wiggles its way down a tube using a traveling wave of bending.

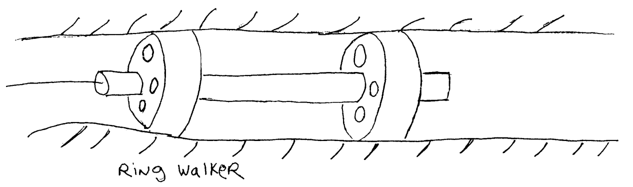

Figure 12: This ring-walker is a piezoelectric inchworm drive which alternately locks, contracts and extends each end.

3.1 Micro Interns

With a team of intern robots, the surgeon can have access to parallel mechanical systems under supervisory control where the supervisor and interns work in a master-slave fashion over a fiber optic or radio link tether. Once this level of teleoperated surgery is established, it is a simple conceptual leap to splicing the tether to geographically dispersed experts around the globe. Thus the right thumb expert in Boston or the left toe expert in Chile can help the same patient in Siberia.

Micromotors and microrobots have high potential in a number of medical procedures. From the GI tract to the vascular system, autonomous machines could act as drug delivery systems, roto-rooters, grinders, markers, artificial sphincters, auxiliary pumps, valves, self-cleaning filters, mobile dams or autonomous endoscopes. Chemical sensors, pressure sensors and flow sensors are now routinely made on silicon microchips and so a little bit of sensing, a little bit of intelligence and a little bit of actuation could be arranged to implement implants that monitor and control flows of various sorts.

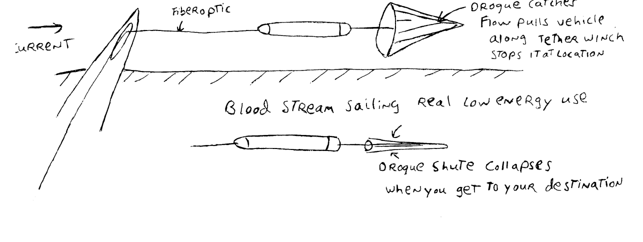

Figure 13: An umbrella-bot sails down the bloodstream reeling out a tether which is locked once the robot reaches the point of interest.

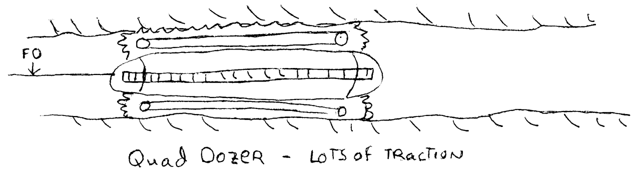

Figure 14: This quad-dozer trundles through pipes while gripping with four tank treads.

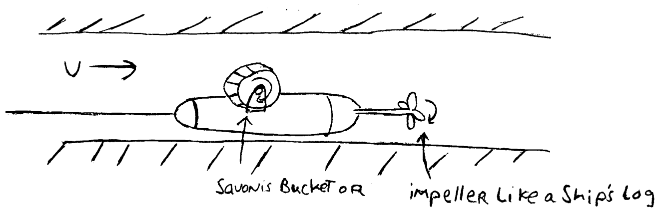

Figure 15: A turbine generates power from the energy supplied by rushing currents.

What will these medical microrobots look like? Figure 11-Figure 14 depict some possible propulsion systems. Manuevering down a tube might be achieved by a traveling wave crawler as shown in Figure 11 or as a piezoelectric inchworm (Figure 12) which alternately locks, extends and contracts to inch its way down a pipe. A form of sailing might propel an umbrella-laden robot along a blood vessel (illustrated in Figure 13), using the flow to push it along and dragging a tether which could be winched in to hold it in place once it has reached its destination. For more rugged terrain, four tank treads equally located around the cylindrical body of a microrobot would find traction by grasping onto the side walls, as shown in Figure 14. For power, miniature batteries could be placed onboard, energy could be supplied through a tether, or perhaps a paddle-wheel generator would tap into the rushing currents as sketched in Figure 15. For cleaning tasks, the demolition-bot shown in Figure 16 would use a simple manipulator for clearing debris.

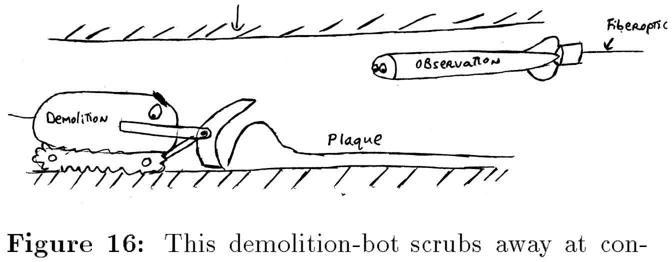

Figure 16: This demolition-bot scrubs away at congesting placque.

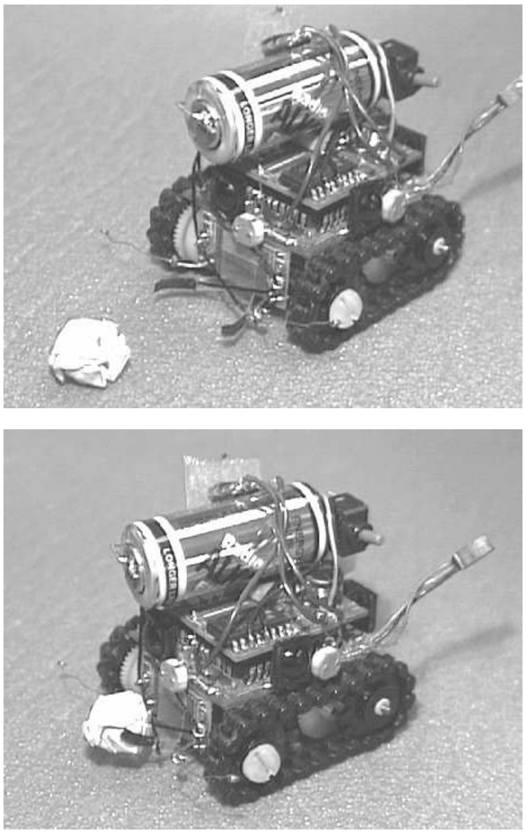

Figure 17: Cleo picking up food. Robot-ant food is a ball of aluminum foil, which is conductive and so can be sensed by the whiskers and continuity test points on the insides of the mandibles.

4 Our State of the Art

Recently, we have developed a highly-integrated autonomous robot which contains many more sensors and actuators than Squirt, in roughly the same volume package. Dubbed Cleo, and illustrated in Figure 17, the robot contains 3 motors, 17 sensors, an onboard computer, gripper, battery and DC-DC converter. The sensors are chosen so as to simulate sensory capabilities of ants and the behaviors programmed into the intelligence system generate ant-like behaviors such as moving towards light and foraging for food.

A number of the sensors used for creating these behaviors can be seen in Figure 17. Four photoresistors for detecting light are mounted on each of the front, back, left and right sides. A near-infrared detector is mounted next to each photoresistor and these are used in communicating moods to other ants. The gripper, or mandible, contains three 'food' sensors, which are simple continuity test points for detecting if aluminum-foil 'food' pellets are present between the claws. Whiskers, which extend out beyond the mandible, detect obstacles or food pellets and are implemented as simple wires running through metal eye-loops, making contact when the whiskers are bent upon bumping an object. Cleo also contains two mandible position sensors, a body-tilt sensor and a low-voltage battery sensor.

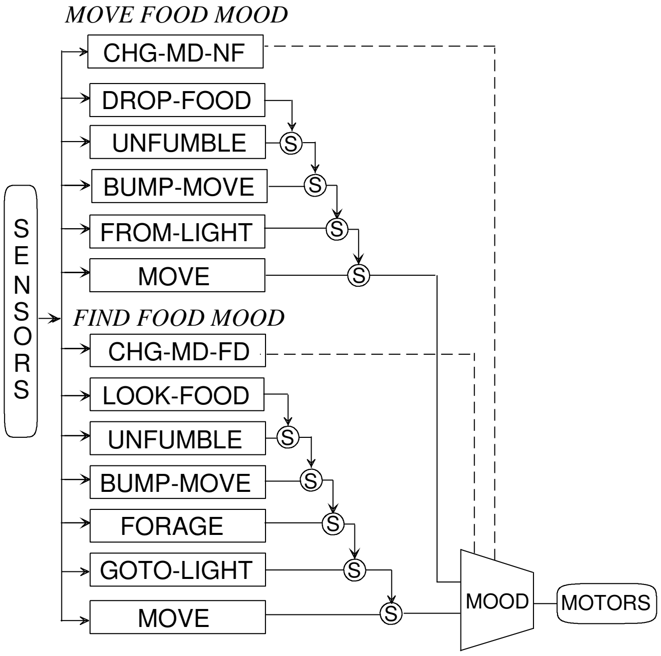

Figure 18: The subsumption architecture diagram of Cleo's intelligence system. With no food in its mandibles, Cleo enters a Find Food Mood. Cleo then moves forward in the direction of maximum light until it bumps into food and then picks it up; putting Cleo in the Move Food Mood.

Cleo's brain is implemented on a Motorola 68HC11E2 microprocessor which contains 256 bytes of random access memory (RAM) and 2K bytes of electrically eraseable programmable read only memory (EEPROM). The subsumption architecture diagram for Cleo's behaviors is shown in Figure 18. The network is composed of finite state machine processes (marked as rectangular boxes) which send messages to one another, to the sensors or to the actuators. Circled-S's signify suppressor nodes, the arbitration mechanism between conflicting behaviors, where higher level behaviors, when activated, can subsume lower level behaviors and enable the outputs from the higher level behaviors to be sent to the actuators.

The example program in Figure 18 initiates the 13 processes shown, which all run in parallel. Depending on the sensory input from the photoresistors, whiskers, food sensors and mandible position sensors, different processes take control for various amounts of time, some processes subsuming others when activated.

When Cleo is turned on, it notices it has no food in its mandibles and begins to look for food. It moves towards light until it finds food, then picks it up and heads away from light until it bumps into a wall, whereupon it drops the food, turns back towards the light, and repeats the process.

In terms of the computational processes illustrated in Figure 18, Cleo's drive motors are directed via commands generated by either the top set of finite state machines or the bottom set, depending on the mood of the robot. The mood is determined by the food sensors. If no food is present in the mandibles, the CHG-MD-NF behavior (change the mood if no food) signals the multiplexor box, marked MOOD, to accept actuator commands generated by the bottom set of behaviors which are labeled as the Find Food Mood. In this scenario, the lowest-level behavior, MOVE, directs Cleo to move forward in a straight line. The GOTO-LIGHT behavior, when initiated by a light level above a certain threshold, directs the robot to move in the direction of maximum light, suppressing straight line motion. After moving for awhile, the robot will eventually hit a wall, whereupon FORAGE is activated and directs the robot to forage for food near a wall, suppressing moving towards light. In a similar manner, BUMP-MOVE causes Cleo to back up when the whiskers detect an obstacle and UNFUMBLE checks the mandible sensors to see if Cleo really is carrying aluminum balls when it thinks it is. If Cleo has fumbled the food, it will try and pick it up again. LOOK-FOOD is a yet higher-level behavior which activates the mandibles to lift the aluminum balls when Cleo senses them in the mandibles.

Once the food sensors and mandible position sensor sense that Cleo is holding the pellets, the CHG-MD-FD (change mood if there is food) behavior signals the multiplexor to begin accepting commands from the top set of behaviors which are labeled as the Move Food Mood. A similar set of actions is then undertaken except that FROM-LIGHT causes Cleo to head away from the brightest sorce of light, and DROP-FOOD directs Cleo to drop its food when it bumps into a wall. CHG-MD-NF then notices that there is no food in the manibles and signals the multiplexor to accept commands from the Find Food Mood processes, and the sequence is repeated.

This subsumption style of programming allows complex robot behaviors to be broken down into simple processes which enables the software to end up fairly lean. All of the behaviors illustrated here and the primitives controlling the sensors and the motors are implemented in just over 1900 bytes of code, small enough to fit in the program space of a single-chip microcontroller.

With clever packaging, the entire robot can fit in the palm of a hand. The final overall size is constrained by the size of the electromagnetic DC motors we presently use from Namiki Corp., which are found in pagers and used as vibration alarms. As pager motors are sold without gears, custom gearboxes have to be fabricated for Cleo. Table II lists the mechanical specifications for Cleo, along with total system power consumption and torque and speed ratings for the Namiki motors.

Table II. Cleo dimensions and power consumption.

Size:	36 mm $\times$ mm 36 mm $\times$ 37 mm
Weight:	34 g
Power:	180 mW
Gear Ratio:	59:1
Gear Box:	4 mm $\times$ 16 mm $\times$ 10 mm
Namiki Motors:	7 mm dia. $\times$ 16 mm
Max Torque:	1.8 gf-cm
No-load Speed:	12,000 rpm

Note that the high no-load speed and low-torque of a DC motor requires significant reduction to drive a vehicle even as small as Cleo.

5 Conclusion

Cleo is a clear demonstration of how an autonomous robot can be made extremely small and yet remain capable of carrying out sophisticated tasks. In addition, Cleo utilizes only conventional off-the-shelf technology. With further advances in miniaturization of actuators and drive systems, we can envision the day when surgeons will have access to far better tools for the medical procedures they need to perform. While Cleo and Squirt are table-top roaming robots, and far from capable of traversing body cavities, engineering efforts steered towards novel locomotion systems, whether they be wriggle-drives, ring-walkers or quad dozers, etc., can be successful. Further miniaturization however, will require technology development in the area of motors. Ultrasonic motors, while promising, require further development. Nevertheless, as technology marches on, it seems tomorrow's surgery will look vastly different than today's.

6 References

[1] Rodney A. Brooks, "New Approaches to Robotics," *Science*, vol. 253, pp. 1227–1232, September 13, 1991.

[2] Rodney A. Brooks, "A Robust Layered Control System for a Mobile Robot," *IEEE Journal of Robotics and Automation*, RA-2, pp. 14–23, April, 1986.

[3] Anita M. Flynn, Rodney A. Brooks, William M. Wells III and David S. Barrett, "Intelligence for Miniature Robots," *Journal of Sensors and Actuators*, vol. 20, pp. 187–196, 1989.

[4] Roger T. Howe, Richard S. Muller, Kaigham J. Gabriel and William S. N. Trimmer, "Silicon Micromechanics: Sensors and Actuators on a Chip," *IEEE Spectrum*, pp. 29–35, July 19, 1990.

[5] Anita M. Flynn, "Gnat Robots (And How They Will Change Robotics)," *Proceedings of the IEEE Micro Robots and Teleoperators Workshop*, Hyannis, MA, November, 1987.

[6] S.C. Jacobsen, R. H. Price, J.E. Wood, T.H. Rytting and M. Rafaelof, "The Wobble Motor: An Electrostatic, Planetary Armature, Microactuator," *Proceedings of the IEEE Micro Electro Mechanical Systems Conference*, Salt Lake City, UT, pp. 17–24, February 20–22, 1989.

[7] David L. Brock, "Review of Artificial Muscle Based on Contractile Polymers," *MIT Artificial Intelligence Laboratory Memo 1330*, November, 1991.

[8] K. Ragulskis, R. Bansevicius, R. Barauskas and G. Kulvietis, *Vibromotors for Precision Microrobots*, Hemisphere Publishing Co., New York, 1988.

[9] Anita M. Flynn, Rodney A. Brooks and Lee S. Tavrow, "Twilight Zones and Cornerstones: A Gnat Robot Double Feature," *MIT Aritificial Intelligence Laboratory Memo 1126*, July, 1989.

[10] Anita M. Flynn, Lee S. Tavrow, Stephen F. Bart, Rodney A. Brooks, Daniel J. Ehrlich, K.R. Udayakumar and L. Eric Cross, "Piezoelectric Micromotors for Microrobots," *IEEE Journal of Microelectromechanical Systems*, vol. 1, no. 1, pp. 44–51, March, 1992.

[11] K.R. Udayakumar, S.F. Bart, A.M. Flynn, J. Chen, L.S. Tavrow, L.E. Cross, R.A. Brooks and D.J. Ehrlich, "Ferroelectric Thin Film Ultrasonic Micromotors," *Proceedings of the Fourth IEEE Workshop on Micro Electro Mechanical Systems*, Nara, Japan, pp. 109–113, Jan. 30–Feb. 2, 1991.

[12] Toshiiku Sashida, "Traveling Wave Ultrasonic Motors," in *Ultrasonic Motors and Actuators*, edited by Akiyama, Chapter 4, Trikepps, in Japanese, 1986.

[13] Kazuya Hosoe, "An Ultrasonic Motor for Use in Autofocus Lens Assemblies," *Techno*, pp. 36-41, in Japanese, May, 1989.

[14] Osamu Kawasaki, Takahiro Nishikura, Yoshinobu Imasaka, Masanori Sumihara, Katsu Takeda and Hiroshi Yoneno, "Ultrasonic Motors," *Denshi Tokyo*, No. 26, 1987.